Chromatic patchy particles: Effects of specific interactions on liquid structure

Oleg A. Vasilyev
Max-Planck-Institut für Intelligente Systeme, Heisenbergstraße 3, Stuttgart, Germany
and IV. Institut für Theoretische Physik, Universität Stuttgart, Pfaffenwaldring 57, Stuttgart, Germany

Boris A. Klumov
Joint Institute for High Temperatures, Moscow, Russia
and L.D. Landau Institute for Theoretical Physics, RAS, 142432, Ac. Semenov 1-A, Chernogolovka, Russia

Alexei V. Tkachenko
Center for Functional Nanomaterials, Brookhaven National Laboratory, Upton, New York, USA
(Received 29 January 2015; revised manuscript received 22 April 2015; published 13 July 2015)

We study the structural and thermodynamic properties of patchy particle liquids, with a special focus on the role of "color," i.e., specific interactions between individual patches. A possible experimental realization of such "chromatic" interactions is by decorating the particle patches with single-stranded DNA linkers. The complementarity of the linkers can promote selective bond formation between predetermined pairs of patches. By using MD simulations, we compare the local connectivity, the bond orientation order, and other structural properties of the aggregates formed by the "colored" and "colorless" systems. The analysis is done for spherical particles with two different patch arrangements (tetrahedral and cubic). It is found that the aggregated (liquid) phase of the "colorless" patchy particles is better connected, denser and typically has stronger local order than the corresponding "colored" one. This, in turn, makes the colored liquid less stable thermodynamically. Specifically, we predict that in a typical case the chromatic interactions should increase the relative stability of the crystalline phase with respect to the disordered liquid, thus expanding its region in the phase diagram.

DOI: 10.1103/PhysRevE.92.012308 PACS number(s): 82.70.Dd, 07.05.Tp, 61.43.Bn

I. INTRODUCTION

In recent years, systems of patchy particles have emerged among the key platforms for advanced self-assembly [1–11]. These are typically micron-scale colloids featuring chemically distinct regions (patches) arranged in a preengineered pattern on the particle surface. In most cases, the patches preferentially bind each other, thus giving rise to strongly anisotropic interparticle interactions, reminiscent of covalent bonding in chemistry. Furthermore, by decorating the patches with single-stranded DNA molecules, one can introduce multiple types of patches as well as a selective type-dependent binding through DNA hybridization [3]. This can be interpreted as "coloring" of patchy particles. One can expect that adding "color" to the directionality of the interactions would lead to a greater control over the resulting morphology.

While the current interest in patchy colloidal systems is motivated primarily by their potential for programmable self-assembly of ordered structures, the study of their disordered phases is of great conceptual importance as well [9,11]. In particular, this provides valuable insights both into the equilibrium phase behavior and kinetics of self-assembly. For instance, Smallenburg and Sciortino [9] have recently demonstrated that the ground state of a system of patchy particles need not be a crystal, even when the particles themselves are highly symmetric. Specifically, for the case of four-patch particles with tetrahedral symmetry, the cubic diamond (CD) crystal becomes the thermodynamically preferred state only in the limit of strong bond directionality, i.e., a very small patch size. Otherwise, the system can achieve its maximum connectivity without sacrificing all of its configurational entropy, and thus preserving the liquid-like order. A similar conclusion was reached independently in our recent study [11]. Rather than exploring the equilibrium phase behavior, we were interested in the structural properties of the random liquid-like aggregate formed from a low density gas of patchy particles. Remarkably the four-patch system demonstrates a relatively high degree of local ordering upon aggregation, as opposed to the six-patch particles with cubic symmetry. We explained this difference by observing that the the coordination number $Z = 4$ is the maximum connectivity of a disordered aggregate under an assumption that the patches are pointlike but the bond directionality is not extreme. Therefore, the four-patch particles may have all their patches connected without forming a crystalline state, in contrast to the six-patch system.

In this work, we expand the previous analysis to study the effects of "chromatic" interactions between the patches on the structural and thermodynamic properties of the liquid phase. One might expect that the bond directionality when combined with the color-based selectivity (e.g., due to DNA functionalization of the patches) should lead to stronger ordering and better programmability of the self-assembled structures [12,13]. As in our previous study, we analyze both 4-patch particles with tetrahedral symmetry (4pch) and 6-patch particles with cubic symmetry (6pch). For each of these systems, we consider two extreme cases: when all the patches are equivalent ("colorless" system), and when all patches that belong to the same particle are of different colors, and their pairwise interactions are subject to a complementarity rule ("colored" system).

II. MODEL AND NUMERICAL ALGORITHM

In our model, we describe a patchy particle as a solid sphere of diameter σ. Patches are located on the surface of this sphere and rotate with it.

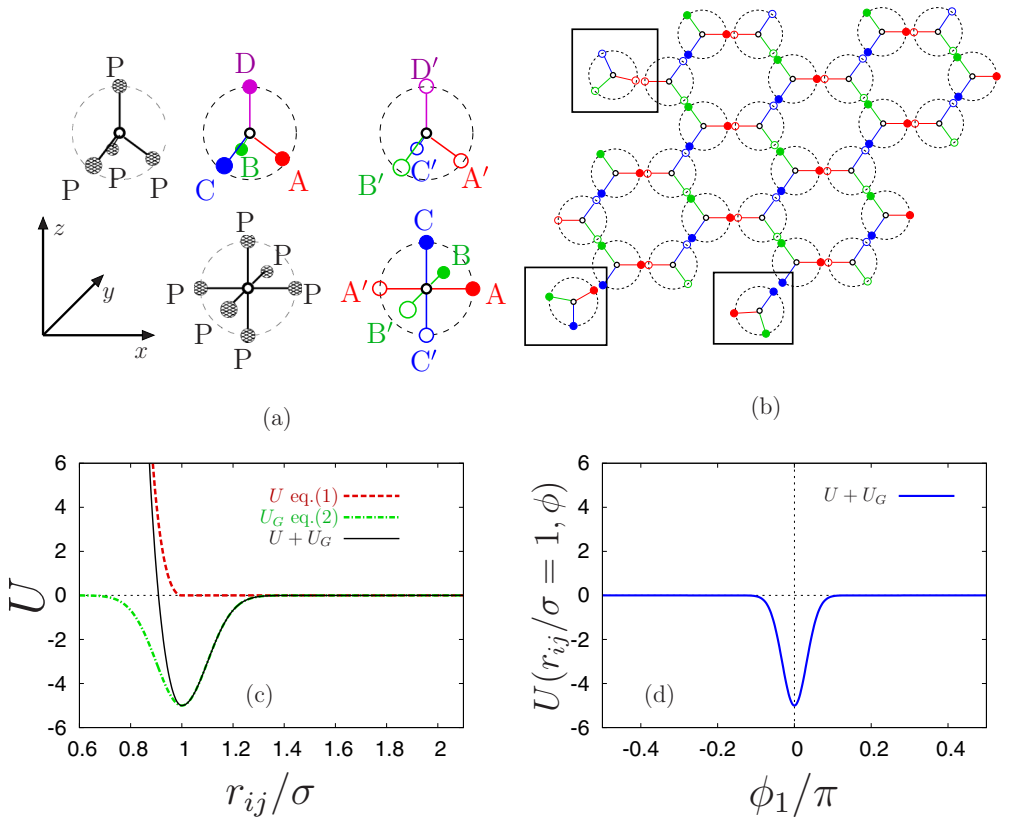

FIG. 1. (Color online) (a) Arrangement of the colorless and colored patches for 4pch and 6pch particles. (b) Top view of a layer of a perfect CD crystal for the colored 4pch system. Particles in black squares do not interact with the aggregate due to the complementarity rule of chromatic interaction. (c) Interaction potentials U [Lennard-Jones core-core repulsion Eq. (1)], U_G [Gaussian patch-patch attraction Eq. (2)] and the total potential $U + U_G$ plotted as functions of the normalized center-to-center distance r_{ij}/σ, for interaction strength $U_p = 5$. (d) The angular dependence of interaction potential U on normalized orientation angle ϕ_1/π of the first particle with respect to the center-center line. The interparticle distance is fixed at $r_{ij}/\sigma = 1$, $U_p = 5$.

The motion of a single particle is represented as a combination of a translational displacement of its center and a rotation of the particle around it. In order to take into account the rotational degrees of freedom, we describe the orientations of the particles with quaternions.

Interactions between the patches satisfy the following rules. In the colored case, only complementary pairs of patches AA', BB', CC', and DD' attract each other. Interactions between other, non-complementary, pairs such as AA, AB', etc., are absent. In the case of colorless particles, every pair of patches PP are mutually attractive.

At the start of simulation, the position of the kth patch of the jth particle with respect to the particle center is given by vector $\mathbf{a}_j^{(k)}(0)$. The system of colored 4pch particles is binary. A "primary" 4pch particle has the following patch positions: $\mathbf{a}_j^{(1)}(0) = (\sqrt{\frac{2}{9}}\sigma, 0, -\frac{1}{6}\sigma)$ (A type), $\mathbf{a}_j^{(2)}(0) = (-\sqrt{\frac{1}{3}}\sigma, \sqrt{\frac{1}{3}}\sigma, -\frac{1}{6}\sigma)$ (B type), $\mathbf{a}_j^{(3)}(0) = (-\sqrt{\frac{1}{3}}\sigma, -\sqrt{\frac{1}{3}}\sigma, -\frac{1}{6}\sigma)$ (C type), and $\mathbf{a}_j^{(4)}(0) = (0,0,\sigma/2)$ (D type). A "complementary" particle is a mirror image of a "primary" one, with patches A', B', C', D' located at the positions A, C, B, D, respectively [see Fig. 1(a)]. For the colored 6pch particle, the complementary patches are located opposite to each other: $\mathbf{a}_j^{(1,2)}(0) = (\pm\sigma/2, 0, 0)$ for A and A', $\mathbf{a}_j^{(3,4)}(0) = (0, \pm\sigma/2, 0)$ for B and B', $\mathbf{a}_j^{(5,6)}(0) = (0, 0, \pm\sigma/2)$ for C and C'.

In our description, vector $\mathbf{r}_j(t)$ represents the position of the particle j at time t. The orientation of that particle is described by unit quaternion $\mathbf{\Lambda}_j(t)$. This quaternion has a form $\mathbf{\Lambda}_j(t) = [\cos(\phi_j/2), \sin(\phi_j/2)\mathbf{n}_j(t)]$, where unit vector $\mathbf{n}_j(t)$ defines the rotation axis passing through the center of the particle and ϕ_j is the angle of rotation around this axis (see, e.g., Ref. [14]).

The location of the kth patch of that particle is therefore given by $\mathbf{a}_j^{(k)}(t) = \mathbf{r}_j(t) + \mathbf{\Lambda}_j(t) \otimes \mathbf{a}_j^{(k)}(0) \otimes \tilde{\mathbf{\Lambda}}_j(t)$. Here $\otimes$ denotes the quaternion product, and $\tilde{\mathbf{\Lambda}}_j(t) = [\cos(\phi_j/2), -\sin(\phi_j/2)\mathbf{n}_j(t)]$ is the corresponding conjugated quaternion.

This quaternion-based approach can be used for molecular dynamic (MD) simulations of rigid objects [15]. There are two types of interactions in our model. Patchy particles repel each other with the following isotropic short-range potential:

$$U(\mathbf{r}_{ij}) = \begin{cases} U_0(\mathbf{r}_{ij}) + (\sigma - |\mathbf{r}_{ij}|)U_0'(\sigma), & \mathbf{r}_{ij} \leqslant \sigma \\ 0, & \mathbf{r}_{ij} > \sigma, \end{cases} \quad (1)$$

where $U_0(\mathbf{r}_{ij}) = 4\epsilon_0[(\sigma/\mathbf{r}_{ij})^{12} - (\sigma/\mathbf{r}_{ij})^6]$ is the standard Lennard-Jones potential, $U_0'(\sigma) = \frac{\mathrm{d}U_0(r)}{\mathrm{d}r}|_{r=\sigma}$ is its derivative, σ is the interaction distance (equivalent to the particle

diameter) as well as cutoff distance, $\epsilon_0 = 1$ is the interaction strength, and $\mathbf{r}_{ij} = \mathbf{r}_i - \mathbf{r}_j$ is the vector connecting the centers of the jth and the ith particles [see Fig. 1(c), dashed line]. The potential is expressed in units of $k_B T$, which is the fundamental energy scale in our problem. In addition to this isotropic interparticle repulsion, the patches that belong to different particles and satisfy complementarity rule (in the colored case) attract each other with a Gaussian potential:

$$U_G\left(\mathbf{a}_{ij}^{(kl)}\right) = -U_p \exp\left[-\left(\mathbf{a}_{ij}^{(kl)}\right)^2/2w^2\right], \tag{2}$$

where $\mathbf{a}_{ij}^{(kl)} = \mathbf{a}_i^{(k)} - \mathbf{a}_j^{(l)}$ is the vector connecting the patch l of the particle j and the patch k of the particle i, $w = 0.2$ is the half-width of the interaction and U_p is the strength of the interaction in units of $k_B T$. In Fig. 1(c) we plot both potentials (for $U_p = 5$) as well as their sum $U + U_G$ (shown by the solid line). The potentials are shown as functions of the normalized distance between the two particle centers r_{ij}/σ for the case when the centers and the attracting patches are located on the same line. The cutoff distance for the Gaussian potential is $5w$. In Fig. 1(d) the angular dependence of potential U is plotted for a fixed interparticle distance, $r_{ij}/\sigma = 1$ [Fig. 1(c) corresponds to $\phi_1/\pi = 0$].

From a known set of displacements and orientations of all particles $\{\mathbf{r}_j, \mathbf{\Lambda}_j\}$ one can compute a set of total forces and torques $\{\mathbf{F}_j, \mathbf{M}_j\}$ acting on them:

$$\begin{aligned} \dot{\mathbf{v}}_j(t) &= \mathbf{F}_j(\{\mathbf{r}_j, \mathbf{\Lambda}_j\})/m \quad & \dot{\mathbf{r}}_j(t) &= \mathbf{v}_j(t) \\ \dot{\omega}_j(t) &= \mathbf{M}_j(\{\mathbf{r}_j, \mathbf{\Lambda}_j\})/I \quad & \dot{\mathbf{\Lambda}}_j(t) &= \tfrac{1}{2}\omega_j(t) \otimes \mathbf{\Lambda}_j(t). \end{aligned} \tag{3}$$

Here I is the moment of inertia, $\dot{\mathbf{v}}_j$ and $\dot{\omega}_j$ are linear and angular accelerations, respectively. All lengths are measured in units of particle radius $\sigma/2$. The mass of a particle is $m = 1$, the moment of inertia of a solid sphere is $I = \frac{1}{10} m\sigma^2 = 0.4$.

We use the Verlet numerical algorithm with the time step $dt = 0.002$ for the numerical integration of Eq. (3). The coupling to a thermal bath is represented by the Langevin noise added to the forces and torques in Eq. (3): $\mathbf{F}_j = -\gamma \mathbf{v}_j(t) + \xi_j(t)$ and $\mathbf{M}_j = -\frac{1}{3}\gamma\sigma^2\omega_j(t) + \zeta_j(t)$. Here $\gamma = 3\pi\nu\sigma$ is the friction coefficient for the solvent viscosity ν. The strengths of delta-correlated noise terms $\xi_j(t)$ and $\zeta_j(t)$ are set by the fluctuation-dissipative theorem: $\langle \xi_i^\alpha(t)\xi_j^\beta(t')\rangle = 2\gamma\delta_{i,j}\delta_{\alpha,\beta}\delta_{t,t'}$, $\langle \zeta_i^\alpha(t)\zeta_j^\beta(t')\rangle = \frac{2}{3}\gamma\sigma^2\delta_{i,j}\delta_{\alpha,\beta}\delta_{t,t'}$. In our units ($\sigma/2 = 1$, $m = 1$, $k_B T = 1$), the friction coefficient γ has a meaning of the diffusion time of a particle over the distance equal to its radius. On the other hand, the time constant $\tau = 1/\gamma$ corresponds to the crossover from the ballistic to the diffusion regime of motion. We set $\gamma = 10$, so that the dynamics of a particle is Brownian on times $t \gg \tau = 0.1$.

In our simulations, the control parameter is the interaction strength U_p. For small values of U_p, the system is in a gas phase; for large values of U_p, it exhibits an aggregation into an amorphous "liquid" phase. We simulate a set of $N = 1000$ particles in a cubic box of size $L = 48$ with periodic boundary conditions. The volume fraction for this system is $\eta = \pi\sigma^3 N/(6L^3) \simeq 0.038$. To verify the robustness of our results, we have performed additional simulations of the "colored" 4pch system for volume fractions twice as large, $\eta \simeq 0.072$, and half the reference value, $\eta \simeq 0.019$. This did not result in any significant variation, aside from the logarithmic shift of the value of U_p at which aggregation is observed, as discussed in Appendix A.

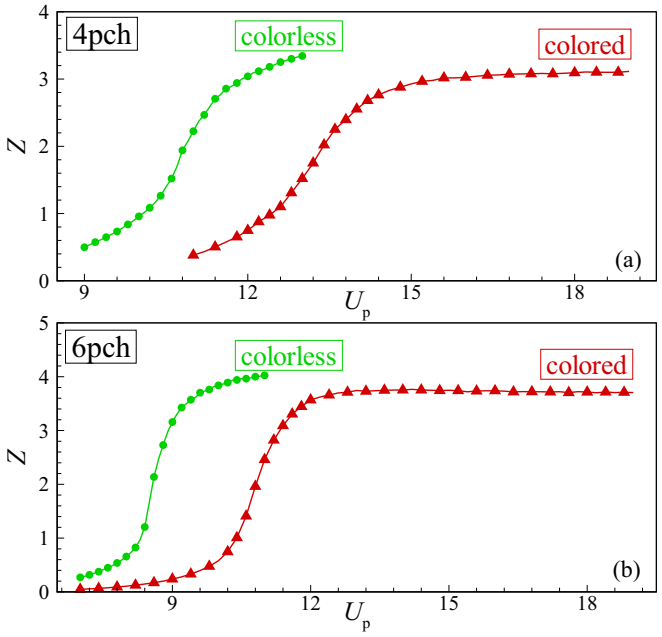

FIG. 2. (Color online) Average number of the topological nearest neighbors Z versus interaction potential U_p for the colored (red triangles) and the colorless (green circles) systems. The data for 4pch and 6pch systems are presented in plots (a) and (b), respectively.

The simulation time is set to $t = 1000$, which is sufficient for most observables to reach their saturation values (the results are averaged over 10 runs). Note that the interpatch binding remains reversible at this time scale, except for very high interaction strength, $U_p > 15$. In Appendix B, we verify the robustness of our results by comparing them to the two alternative protocols, in which U_p is gradually increasing or decreasing, both of which have a longer integration time, $t = 10\,000$. That shifts the threshold of the irreversible binding further up, to $U_p \simeq 17$, but does not lead to any alteration to the results reported in this work.

III. RESULTS AND ANALYSIS

A. Topological characterization

Two patches are considered to be bound if the distance between their centers is less than the half-width $w = 0.2$. We define a pair of particles to be topological nearest neighbors (NNs) if there is such a bond formed between their patches. This definition is robust with respect to the choice of the threshold length w since the interacting patches are strongly localized relative to each other. The computed values of the mean coordination number Z (i.e. the number of NNs) are plotted in Fig. 2 versus interaction strength U_p, for 4pch (a) and 6pch (b) systems. As U_p increases, all the systems undergo transitions from a gas to an amorphous aggregate.

From the thermodynamic point of view, the instability of the uniform gas of particles towards the formation of a dense aggregate corresponds to its spinodal decomposition. When this occurs, the aggregate is essentially an early liquid phase. The reversibility of the interparticle bonding (at $U_p < 15$)

implies that the local structure of the aggregate is similar to the bulk liquid. It should be noted, however, that the relaxation of clusters to spherical droplet shapes is a much slower process not captured in our study. In view of this, and due to the finite system size, there is always an interfacial correction to any of the thermodynamic observables reported below. Partially because of this limitation, we do not use our data to directly compare the thermodynamics of the liquid and crystalline phases. Instead, we are focused on a specific aspect of the problem: the effect of chromatic interactions on structural and thermodynamic properties of the liquid.

The aggregation is reflected by a gradual change of the coordination number from 0 (unbound particles), to a certain saturation value Z_0. The latter is the characteristic of the liquid phase and its value depends on the system. In particular, both colored and colorless 6pch particles form aggregates with Z_0 close to 4 (4.2 and 3.8, respectively). 4pch systems exhibit a somewhat lower connectivity: $Z_0 \simeq 3.2$ for the colored and $Z_0 \simeq 3.5$ for the colorless one.

The intermediate values of the mean NN number correspond to the coexistence of the condensed liquid phase with a gas of single particles and smaller clusters. All these cases support our earlier argument that the coordination number $Z_0 = d + 1$ plays a special role for a patchy liquid in d-dimensional space [11]. This value emerges from the comparison of the number of mechanical constraints with the number of translational degrees of freedom. The rotational degrees of freedom are not taken into account in this counting since a much stronger patch-patch localization is required in order for them to be frozen. The fact that Z_0 is somewhat below 4 for 4pch system is also natural as $Z = 4$ is the maximum possible number of bonds for these particles, and some of the patches remain unbound, especially for the colored system. One could expect $Z = 4$ to be reached in the limit of very strong attraction, but that regime is not accessible partially because of the finite size effects, and also since the binding becomes nearly irreversible on the time scale of the simulations when the interactions are stronger than the threshold value, $U_p \simeq 15$.

Another mechanism that partially explains the incomplete binding of 4pch particles deals with a finite angular rigidity of the patch-patch bond. In our general argument presented in Ref. [11], we obtained the result $Z = 4$ in the limit when angular constraints are completely relaxed. They are indeed harder to arrest compared to the translational ones in a generic case, yet the angular rigidity remains finite. This rigidity leads to lowering of Z_0 in the liquid phase, as reported in Ref. [16].

B. Chromatic effect on thermodynamics

The colored patchy particles exhibit aggregation at a significantly higher interaction strength U_p than the corresponding colorless ones. Coexistence of the liquid-like aggregate with the gas of particles implies that the chemical potential is the same in both phases. Therefore, onset of the condensation approximately corresponds to the point at which the chemical potential of the free particle gas, $\mu_0 = k_B T \ln \eta$ is equal to that of the liquid phase. The shift of the aggregation curves, ΔU_p, between the colorless and the corresponding colored system shown in Fig. 2, can be related to the difference in the chemical potential $\Delta\mu$ between the two aggregates, taken at the same interaction potential. Indeed, $\Delta\mu$ should be offset by the difference in the interaction energy per bond:

$$\frac{\Delta\mu}{k_B T} = \frac{Z_0}{2}\Delta U_p \ . \tag{4}$$

Here $\frac{Z_0}{2}$ is the average number of bonds per particle in the aggregate.

This estimate gives $\Delta\mu \simeq 4k_B T$ for both 4pch and 6pch systems. More reliably the free energy of the aggregated phase can be found by the thermodynamic integration [17]:

$$F = \int_0^{1/k_B T} \frac{E(\beta k_B T U_p)\, d\beta}{\beta} = \int_0^1 \frac{E(xU_p)\, dx}{x} \ . \tag{5}$$

Here $E(U_p)$ is the ensemble averaged potential energy per particle, and F is the Helmholtz free energy per particle. The uniform gas phase that corresponds to $U_p = 0$ is chosen as a reference state, $F = 0$.

In the case of chromatic 4pch system, the system is binary with 1:1 composition. This means that the reference free energy of this particular system contains additional mixing entropy contribution, $-k_B T \ln 2$. As will be shown below, it does not lead to any physically measurable effect as long as the composition of all phases discussed remains the same. In this calculation we took into account the fact that U_p is expressed in units of $k_B T$. We ignore the kinetic energy contribution to F since it is completely decoupled from any structural transformation in nonquantum systems.

The chemical potential μ can be calculated as the Gibbs free energy per particle. In the limit of a completely aggregated state (high value of U_p), the pressure coming from the dispersed particles can be neglected, and the Helmholtz and Gibbs free energies become identical; i.e., $F = \mu$. According to the results of thermodynamic integration, presented in Fig. 3, the chemical potential of the colored aggregate is increased with respect to the colorless one by an amount well described by a linear function of U_p:

$$\Delta\mu = \Delta F = \Delta_0 + 0.17 k_B T U_p. \tag{6}$$

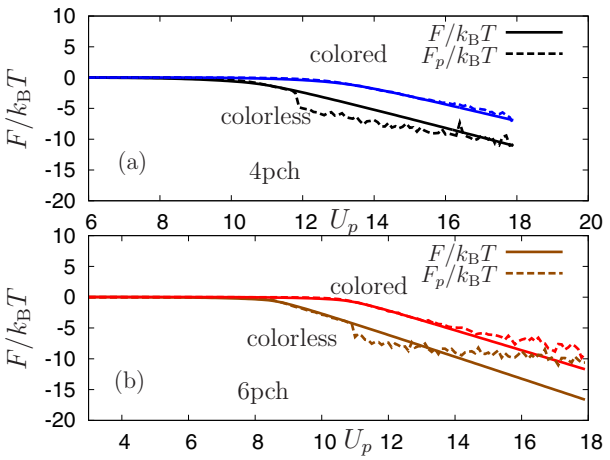

FIG. 3. (Color online) Helmholtz free energy per particle F calculated by the thermodynamic integration and $F_p = 1 + \ln(p) - p$ (in $k_B T$ units) plotted as functions of U_p, for the colored and the colorless systems of (a) 4pch and (b) 6pch particles.

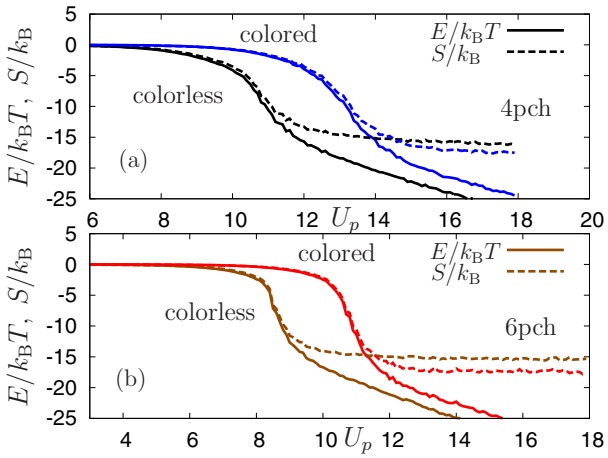

FIG. 4. (Color online) Comparison of the energy per particle E (in k_BT units) and the entropy per particle S (in k_B units) plotted as functions of U_p for the colored and the colorless systems of (a) 4pch and (b) 6pch particles.

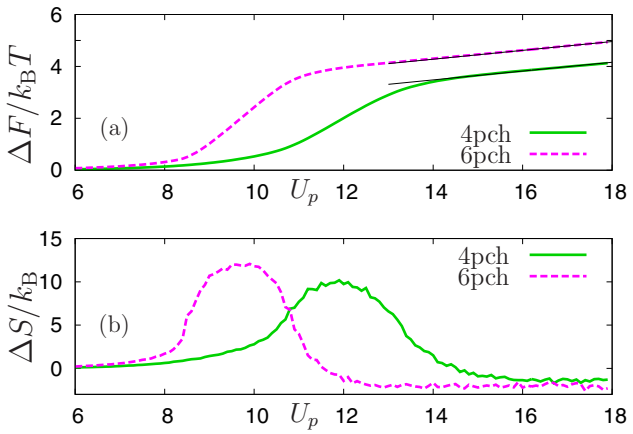

FIG. 5. (Color online) (a) The difference ΔF (in k_BT units) between the Helmholtz free energy per particle of the colored and colorless systems vs U_p, for 4pch and 6pch particles. (b) The difference ΔS (in k_B units) between the entropy per particle of the colored and colorless systems vs U_p, for 4pch and 6pch particles.

Here $\Delta_0 \simeq 1.1k_BT$ for 4pch and $\Delta_0 \simeq 1.9k_BT$ for 6pch. In both of these cases, this "chromatic" correction is close to $4k_BT$ near the aggregation point, in a good agreement with our earlier rough estimate. Note that we do not include here the additional contribution due to mixing entropy of the chromatic 4pch system, $-k_BT \ln 2$, that has been adsorbed in the corresponding reference free energy.

Our integration procedure is further verified in Appendix B. Furthermore, the result of integration can be independently related to the fraction of particles in the gas phase, p. Namely, the chemical potential of a gas of unbound particle can be expressed in terms of their volume fraction, $p\eta$ as $\mu = k_BT \ln(p\eta)$. The Helmholtz free energy per particle differs from the chemical potential by the amount PV/N, where pressure P is proportional to the number density of all the dispersed objects, including the individual particles and the bigger clusters. In the regime when this correction is relevant (i.e., of the order of k_BT), the pressure is dominated by the contribution from the gas of single particles, $P = pNk_BT/V$. Therefore, $\mu - F = PV/N = pk_BT$. This leads to an alternative expression for F:

$$F_p = k_BT[\ln(p) - p + 1]. \quad (7)$$

Here we have subtracted the Helmholtz free energy of the uniform gas phase, to keep the same reference state as in Eq. (5). While this method is significantly less accurate than the thermodynamic integration (as can be seen in Fig. 3), it provides an additional verification for our results.

One can also separate the entropic and energetic contributions to the chromatic free energy correction, Eq. (6), by noting that $TS = E - F$. The corresponding data are presented in Fig. 4. For both 4pch and 6pch systems, the entropic correction TS reaches a constant value very close to the corresponding parameter Δ_0 in Eq. (6). Hence, the linear term represents the energy correction, due to the lower number of NNs in the colored case. Within this interpretation, the coefficient 0.17 should be close to $\Delta Z_0/2$, implying that $\Delta Z_0 \simeq 0.35$ is the difference in the mean coordination number between the respective colored and colorless systems. The value of this parameter is indeed consistent with the data in Fig. 2. The free energy difference ΔF (in k_BT units) and the entropy difference ΔS (in k_B units) for the colored and colorless systems are plotted in Fig. 5.

C. Comparison to crystal phase

The computed effect of the chromatic interactions on the thermodynamics of the liquid phase can be compared to the similar effect expected in the crystal phase. Note that the colored and colorless systems when arranged into an ideal crystalline configuration are locally indistinguishable: they have the same ground state energy and the same vibrational modes, unless the coloring is inconsistent with the given crystal lattice. Therefore, the only difference in their free energies is due to configurational entropy. Specifically, that the colorless particles have a larger number of equivalent orientational states that would preserve the bonds with their neighbors. There are 12 such orientations of a colorless 4pch particle and 24 for the case of 6pch system. The resulting difference in the chemical potential between the colorless and colored system is purely entropic, $k_BT \ln 12 \simeq 2.5k_BT$ and $k_BT \ln 24 \simeq 3.2k_BT$, respectively. Since the colored 4pch system is binary, there is again an additional mixing entropy correction $-k_BT \ln 2$ in that case. This constant addition is identical to the one previously adsorbed in the reference free energy of the corresponding liquid phase. Therefore, it does not lead to any physical effect, and can be simply dropped in the present analysis. This is indeed expected, as long as the composition of the system remains the same.

On the one hand, this entropic correction is greater than that computed for the corresponding liquid phases ($\Delta_0 \simeq 1.1k_BT$ and $\Delta_0 \simeq 1.8k_BT$). However, this entropic effect is easily offset by the energy difference. Indeed, according to Eq. (6), $\Delta\mu$ becomes greater that the corresponding correction for the crystal ($2.5k_BT$ and $3.5k_BT$ respectively) once the interaction parameter exceeds $U_p \simeq 8$. While the parameter itself is model specific, this interaction strength is definitely insufficient to

condense the dispersed particle system even at the relatively high volume fraction used in our simulations.

We therefore expect that in a generic case where the patch-patch interaction is sufficient for the aggregation of a dilute colloidal suspension, the ordered phase will gain additional stability due to the chromatic interactions. In other words, if we start with the colorless system, and make the patches colored with the color-specific binding, this would lead to free energy penalty both to the crystal and liquid phases, but the latter penalty would be greater. The colored and colorless systems are certainly physically distinct, so these free energy differences are not directly measurable. However, we use the gas phase at the same concentration as a reference state for all the cases, which allows us to determine the effect of coloring on the relative stability of the liquid and crystal phases.

It should be emphasized that we do not perform a direct comparison of the liquid to the crystal, instead we only evaluate the strengths of the chromatic effects for each of the phases separately. While the one for the crystal is obtained based on an analytic argument, the effect on the bulk liquid is extracted from our MD simulations and therefore may have errors coming from interfacial effects. One can estimate the role of the interface by noting that the average coordination number of colorless 4pch aggregate, $Z_0 = 3.5$ deviates from its maximum possible value 4 by approximately 10%. This sets an upper bound on the strength of the interfacial or finite size correction to the overall free energy when compared to the bulk liquid. We therefore expect that the presence of an extended interface should result a similar correction to the chromatic effect itself. Such a correction would not alter our main conclusions in any significant manner.

D. Local connectivity and correlations

Figure 2 indicates only a modest difference in the maximum values of the mean coordination number Z between the colored and colorless systems. However, the detailed analysis of its PDFs reveals a much greater qualitative contrast. Figures 6 and 7 show the influence of the color of the patches on the distribution of the number of NNs for 4pch and 6pch systems, respectively. As interaction strength U_p increases, the systems form amorphous aggregates [11] with nearly constant distributions of the topological NNs. This transition is clearly seen in Figs. 6 and 7 for all four cases.

The colored 4pch system is dominated by particles with $Z = 3$, while its colorless counterpart has a much larger fraction of particles with completely saturated bonds, i.e., $Z = 4$. This must be a result of additional constraints imposed by the coloring of the patches. A similar trend, although not as pronounced, is also seen for the 6pch particles.

An alternative characterization of the local structure in the aggregated liquid phase is provided by the radial distribution function $g(r)$, shown in Fig. 8 for the 4pch and 6pch systems, both colored (red curves) and colorless (green curves). Additionally, the average number of particles inside of a sphere of radius r, $N(<r) \equiv 3\eta \int_0^r \xi^2 g(\xi)\, d\xi$, are presented on the same plots. There is a clear correspondence between the topological NNs discussed above, and the geometrical NNs represented by the first peak in $g(r)$: their number is also close to $Z = 4$, and it is slightly lower for the colored system than for the

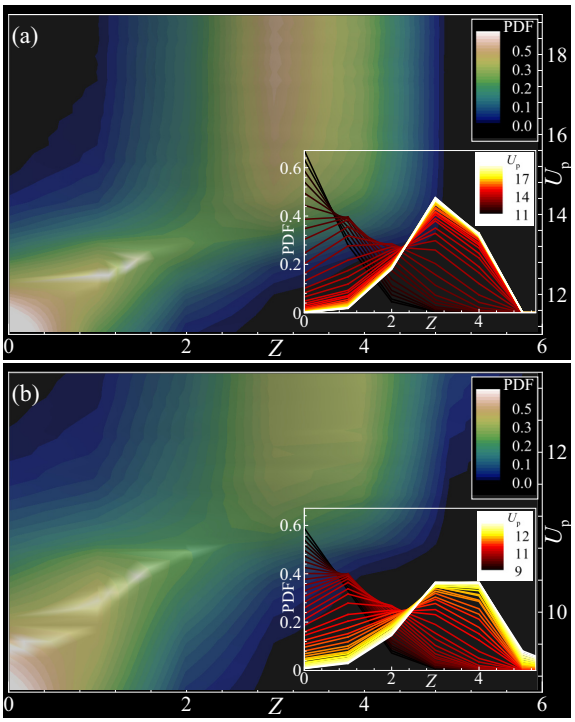

FIG. 6. (Color online) The probability distribution function (PDF) of the coordination number Z at variable interaction strengths U_p (vertical axis). Plots (a) and (b) represent the colored and colorless 4pch systems, respectively. The insets show the same PDFs at selected values of U_p (the bright color corresponds to the strongest attraction).

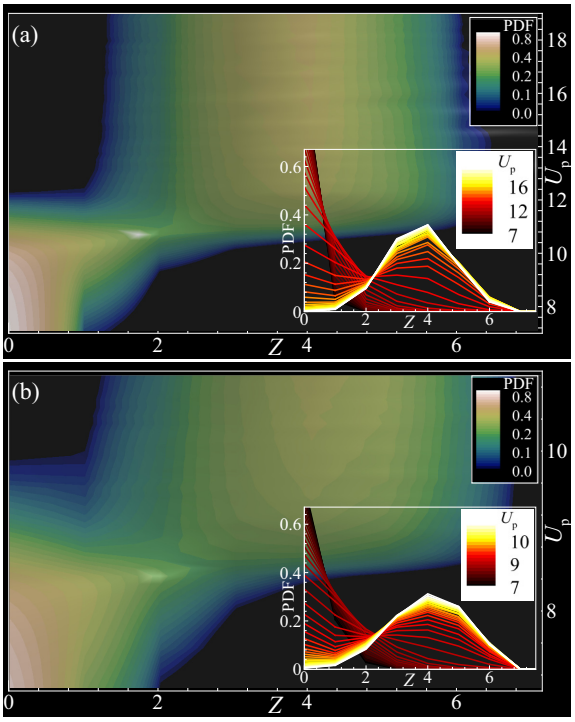

FIG. 7. (Color online) The probability distribution function (PDF) of the coordination number Z at variable interaction strengths U_p (vertical axis). Plots (a) and (b) represent the colored and colorless 6pch systems, respectively. The insets show the same PDFs at selected values of U_p (the bright color corresponds to the strongest attraction).

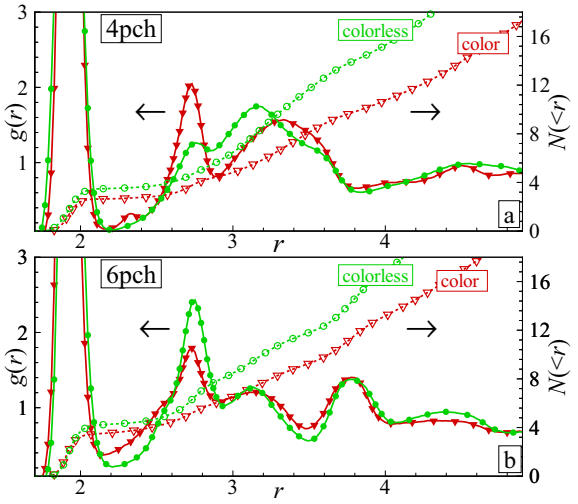

FIG. 8. (Color online) The radial distribution function (RDF) $g(r)$ showing the mean number of particles inside the sphere of radius r plotted for colored (red filled triangles) and colorless (green filled circles) and the corresponding cumulative function $N(<r)$ ($N(<r) \equiv 3\eta \int_0^r \xi^2 g(\xi)\, d\xi$) for colored (red empty triangles) and colorless (green empty circles) for liquid-like systems 4pch (a) (potential values are $U_p = 18$ for colored and $U_p = 13$ for colorless systems) and 6pch (b) (potential values are $U_p = 18$ for colored and $U_p = 11$ for colorless systems) for the volume fraction fraction $\eta = 0.038$. It is clearly seen that the colorless patchy systems form denser aggregates than the colored ones.

colorless one. The analysis of the cumulative curves reveals that aggregates of the colorless patchy particles are somewhat denser than those of colored ones, which is consistent with our observation that they are also more connected.

E. Orientational order

To further characterize the local structural properties of the patchy system, we use the bond orientational order parameter method [18], which has been widely used in the context of condensed matter physics [18], hard sphere [19–21] and Lennard-Jones systems [22–25], complex plasmas [26–29], colloidal suspensions [30,31], metallic glasses [32], confined films [33,34], granular media, etc. Within this method, the rotational invariants of rank l of both the second $q_l(i)$ and the third $w_l(i)$ order are calculated for each particle i in the system from the vectors (bonds) connecting its center with the centers of its $N_{\rm nn}(i)$ nearest neighboring particles

$$q_l(i) = \left[\frac{4\pi}{(2l+1)} \sum_{m=-l}^{m=l} |q_{lm}(i)|^2 \right]^{1/2} \tag{8}$$

$$w_l(i) = \sum_{\substack{m_1,m_2,m_3 \\ m_1+m_2+m_3=0}} \begin{bmatrix} l & l & l \\ m_1 & m_2 & m_3 \end{bmatrix} q_{lm_1}(i) q_{lm_2}(i) q_{lm_3}(i), \tag{9}$$

where $q_{lm}(i) = N_{\rm nn}(i)^{-1} \sum_{j=1}^{N_{\rm nn}(i)} Y_{lm}(\mathbf{r}_{ij})$, Y_{lm} are the spherical harmonics and $\mathbf{r}_{ij} = \mathbf{r}_i - \mathbf{r}_j$ are the vectors connecting the centers of particles j and i. We note that the bond order parameters w_l scale as $w_l \propto q_l^3$; so, in general, these parameters are much more sensitive to the local orientational order in comparison with q_l. Here, to define structural properties of patchy particles, we calculate the rotational invariants q_l, w_l for each particle that has the maximum number of NNs: $Z = 4, 6$, respectively. The first shells of the ideal 4pch and 6pch systems correspond to the cubic diamond (CD) and the simple cubic (SC) arrangements, respectively.

TABLE I. Rotational invariants for perfect patchy crystals.

System	Structure	q_4	q_6	w_4	w_6
4pch	CD (1st shell, 4 NNs)	0.509	0.628	−0.159	−0.013
6pch	SC (1st shell, 6 NNs)	0.76	0.35	0.159	0.013

The values of the corresponding rotational invariants q_l and w_l for the perfect patchy crystals are shown in Table I.

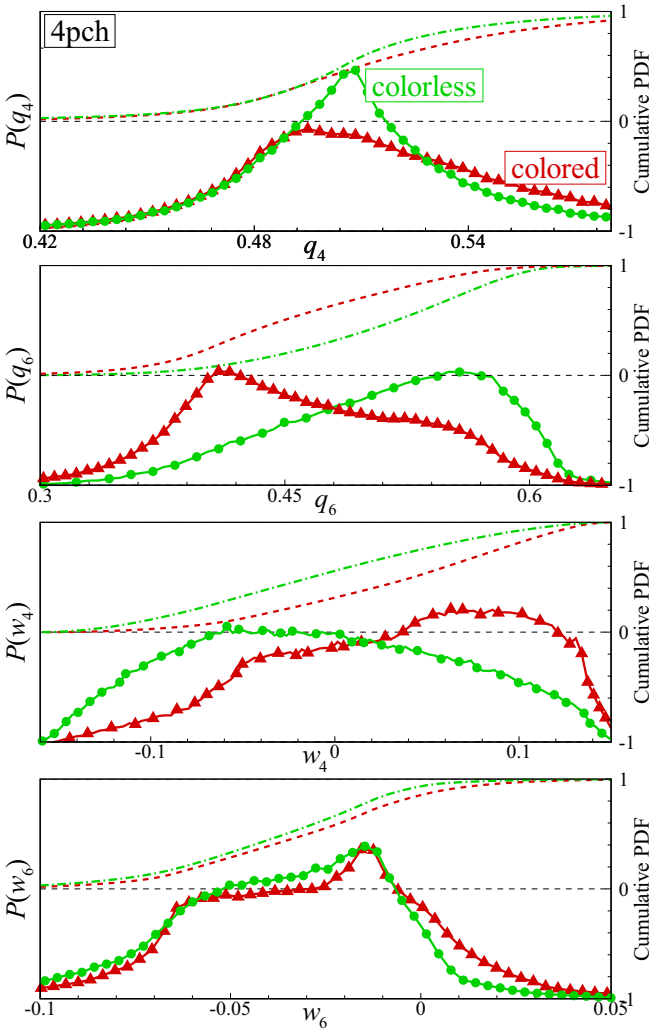

FIG. 9. (Color online) Patchy system 4pch. Probability distribution functions $P(q_l)$ and $P(w_l)$ of different rotational invariants q_l and w_l ($l = 4,6$), calculated for particles with exactly $Z = 4$ topological NNs. PDFs are plotted both for the colored (red triangles, for $U_p = 18$) and colorless (green circles, for $U_p = 13$) patchy systems in the aggregated phase at the standard volume fraction $\eta \simeq 0.038$. Corresponding cumulative functions of probability distributions are plotted by red dashed line and green dash-dotted line for colored and colorless cases, respectively.

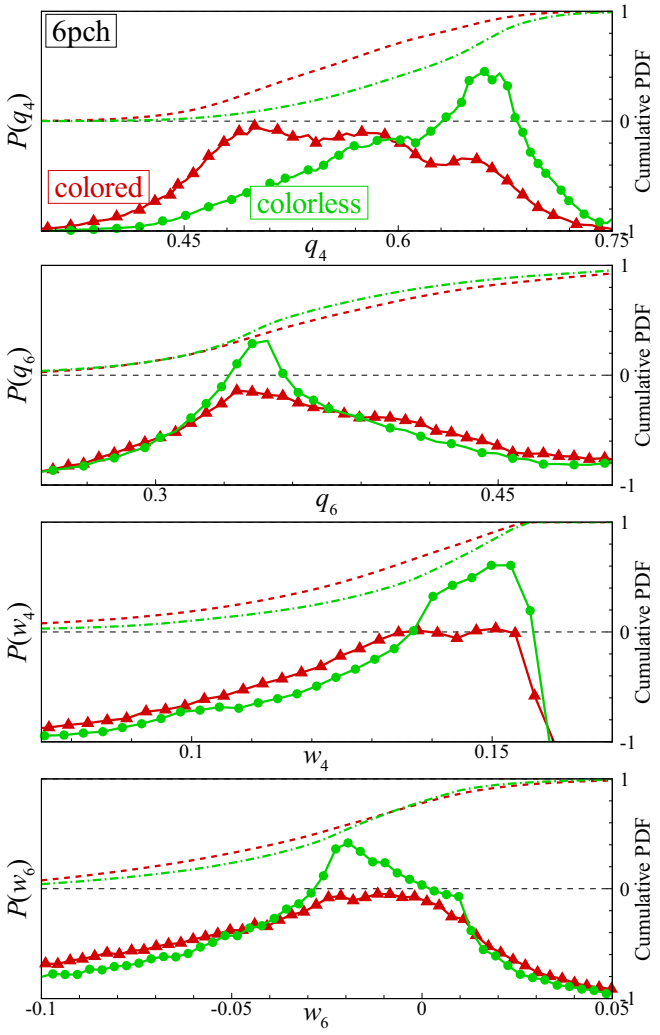

FIG. 10. (Color online) Patchy system 6pch. Probability distribution functions $P(q_l)$ and $P(w_l)$ of different rotational invariants q_l and w_l ($l = 4,6$), calculated for particles with exactly $Z = 6$ topological NNs. PDFs are plotted both for the colored (red triangles, $U_p = 18$) and colorless (green circles, $U_p = 11$) patchy systems in the aggregated phase at the standard volume fraction $\eta \simeq 0.038$. Corresponding cumulative functions of probability distributions are plotted by red dashed line and green dash-dotted line for colored and colorless cases, respectively.

The characterization of the local bond orientation order for 4pch and 6pch aggregates is presented in Figs. 9 and 10, respectively, both for the colored (triangles) and the colorless (circles) cases. The probability distribution functions $P(q_l)$ and $P(w_l)$ of the rotational invariants q_l and w_l ($l = 4,6$), and their cumulative distributions shown in the figures, reveal that the colorless systems are more ordered than the colored ones. Specifically, for the colorless system the PDFs exhibit broad yet pronounced peaks at the locations expected for the corresponding perfect crystal. The colored liquid is significantly less ordered, which is in a general agreement with the observation that it is less connected and more frustrated due to the color constraints, and with the fact that it is less stable thermodynamically.

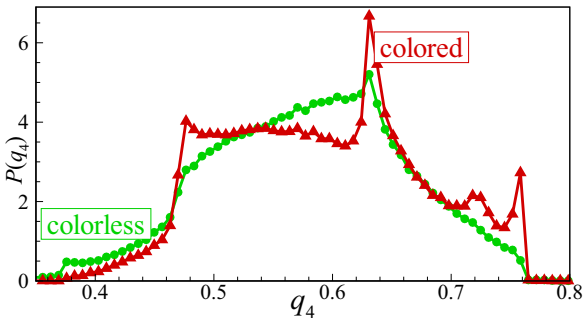

FIG. 11. (Color online) Patchy system 4pch. Probability distribution function $P(q_4)$ calculated for particles with exactly $Z = 3$ topological NNs, both for the colored (red triangles, for $U_p = 18$) and colorless (green circles, for $U_p = 13$) systems in the aggregated phase for the volume fraction $\eta = 0.038$. Note the strong peaks indicating better local ordering of the colored system, in striking contrast with the results obtained from the analysis of fully connected particles with $Z = 4$, in Fig. 9.

This mostly coherent picture is however challenged when we analyze the local bond orientation order for the subset of 4pch particles with a smaller number of NNs, $Z = 3$. In particular, we distinguish a striking example of $P(q_4)$ that indicates remarkable enhancement of the local order in the colored system compared to the colorless one (see Fig. 11). A possible explanation of this anomaly is that additional bonds in the colorless system come at the expense of deformation of the network, and the resulting strain affects weaker connected $Z = 3$ nodes more strongly than those with $Z = 4$. Indeed, if we imposed a condition that each interparticle bond is perfectly aligned with the vector pointing towards the center of the patch, the maximum average coordination number that could be achieved would be $Z = 5/3$. As we have discussed in our earlier work [11], this constraint is typically unrealistic, and the coordination number is expected to be larger (tending towards $Z = 4$, consistently with the present results). These additional bonds however do result in a modest bond rotation and strain in the particle network. Presumably, this leads to the suppression of local order near $Z = 3$ particles in the better connected colorless system.

IV. CONCLUSIONS

The central conclusion of our study is that the colored patches provide an important additional element of control over the self-assembled structures. In our work, we considered the early stages of liquid formation from a gas of patchy particles, both colored and colorless. We analyzed the structural and thermodynamic properties of the aggregated phase and concluded that the colorless patchy systems are typically more connected, denser and more ordered than the corresponding colored ones. The only identified anomaly that goes against this general trend deals with the local bond orientation order near 4pch particles with coordination number $Z = 3$. That type of order is noticeably increased when the chromatic interactions are introduced.

By means of thermodynamic integration, we were able to compute the chromatic correction to the chemical potential of the aggregated phase, which we treat as a model for the bulk

liquid. On the other hand, we evaluated a similar correction to the crystal phase based on an analytic entropic argument. By comparing the two results, we predict that in a generic case, the chromatic interaction between patches would lead to a greater free energy penalty for the disordered liquid phase than for the corresponding ordered structure. This implies an enhanced stability of crystals made of the colored patchy particles compared to the uncolored ones. In particular, we expect that the limitation on the patch size required for the crystallization according to Ref. [9] would be less severe in the chromatic case.

The chromatic interactions discussed in this work may be employed not only to shift the balance in the order-disorder transitions, but also to select a desired self-assembled structure in the case of crystalline polymorphism. The classical example of that kind is the competition between cubic and hexagonal diamond lattices (CD and HD), both of which have identical tetrahedral arrangement of NNs. It is an attractive idea to select a specific lattice by chromatic patch-patch interactions. Unfortunately, our binary system of 4pch particles does not provide sufficient control for that both CD and HD are possible with the same set of particles. However, it should be possible to control the outcome in polymorphic system if more than two particle types are used. This constitutes an intriguing conceptual problem for future study.

ACKNOWLEDGMENTS

This study is supported by European Research Council under FP7 IRSES Marie-Curie grants PIRSES-GA-2010-269139 and PIRSES-GA-2010-269181. Research carried out in part at the Center for Functional Nanomaterials, Brookhaven National Laboratory, which is supported by the U.S. Department of Energy, Office of Basic Energy Sciences, under Contract No. DE-SC0012704. Structural analysis was supported by the Russian Science Foundation, Project No. 14-12-01185. Numerical simulations were supported by the Russian Science Foundation, Project No. 14-50-00124.

APPENDIX A: EFFECT OF THE OVERALL VOLUME FRACTION

To verify the robustness of our results, we varied the overall volume fraction of the particles. Specifically, the simulations of 4pch colored system were conducted at $\eta = 0.019, 0.038, 0.076$ ($N = 500, 1000, 2000$ particles, respectively, for the same system size $L = 48$) In Fig. 12 we plot the resulting energy E and Helmholtz free energy F per particle (in $k_B T$ units), as a function of interaction potential U_p.

As one can see from the plots, the change in volume fraction leads to a shift of the onset of aggregation. At a relatively low value of U_p, when aggregation starts, the monomers coexist with dimers and some larger clusters. As long as these clusters are not large enough to contain any loops, the number of particles N determines the number of bonds, $N - 1$. Therefore, the relative fractions of these small clusters scale as $\eta^{(N-1)} \exp[-(N-1)U_p]$. Hence, the composition of the system in this early aggregation regime is invariant with respect to a simultaneous renormalization of the volume fraction, $\eta \to A\eta$, and the logarithmic shift in U_p: $U_p \to U_p - \ln(A)$. In the opposite limit, when the interaction becomes strong, thermodynamic parameters such as average energy per particle are dominated by the properties of the aggregated (liquid) phase, and therefore invariant with respect to the change in η. Both the logarithmic shift and the asymptotic convergence at high value of U_p are indeed observed in our numerical data for $E/k_B T$.

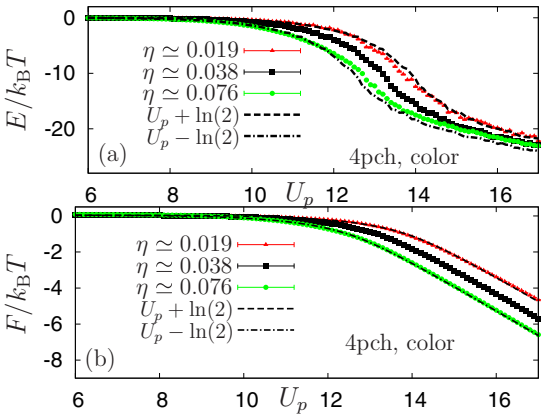

FIG. 12. (Color online) Results for three different values of the volume fraction $\eta = 0.019, 0.038, 0.076$ (triangles, squares, and circles, respectively) for colored 4pch system. We also plot the result for $\eta = 0.038$ shifted to right $U_p = U_p + \ln 2$ (dashed line) and to left $U_p = U_p - \ln 2$ (dash-dotted line). (a) The energy of the system E per particle (in $k_B T$ units) plotted as a function of U_p; (b) Helmholtz free energy per particle F calculated by the thermodynamic integration and (in $k_B T$ units) plotted as functions of U_p.

For comparison we plot the graph for $\eta = 0.038$ shifted to $\ln 2$ left (dash-dotted line) and right (dashed line).

APPENDIX B: ALTERNATIVE SIMULATION PROTOCOLS

Our thermodynamic integration procedure is potentially problematic due to an underlying gas-to-liquid transition.

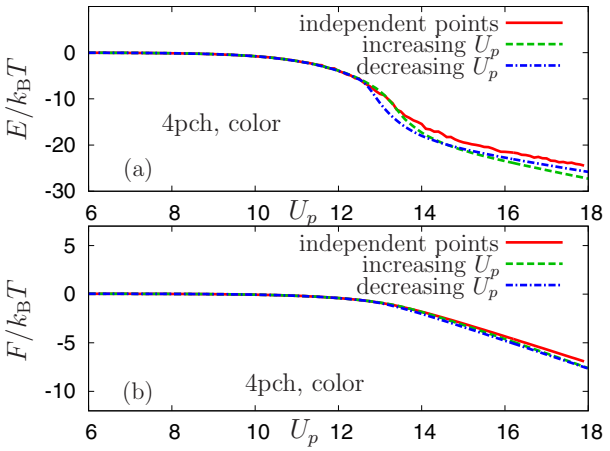

FIG. 13. (Color online) Dependence of results on the way of the system equilibration: for independent simulation of each potential U_p point (solid line), for sequential increasing of potential (dashed line) and sequential decreasing of potential (dash-dotted line). (a) The energy of the system E per particle (in $k_B T$ units) plotted as a function of U_p; (b) Helmholtz free energy per particle F calculated by the thermodynamic integration and (in $k_B T$ units) plotted as functions of U_p.

However, this transition in the N,V ensemble occurs in a continuous manner, with the fraction of the aggregated (liquid) phase growing from 0 to 100%. The preformed small clusters play role of nucleation centers in this transition. Nevertheless, the potential for residual kinetic effects remains, and it is important to make sure that they do not affect our results. In order to verify this, we performed additional numerical studies in which the original protocol was altered.

The result reported in the main text were obtained by a series of independent simulations of the system at various fixed values of potential U_p (the simulation time $t = 1000$ for each point, averaged over 10 independent runs). The two alterations to this protocol are presented here. First, we start from zero potential $U_p = 0$ and gradually increase the interaction potential to $U_p = 20$. In a second set of simulations, we started at $U_p = 20$ and then gradually decrease it to zero. The simulation time for each intermediate value of U_p was $t = 10\,000$, and the averaging was performed over 100 independent series of increasing or decreasing sets.

In Fig. 13(a) we plot results for the energy per particle for all three protocols. There is a slight variation between them, and a hint of hysteretic behavior. Nevertheless, they are not strong enough to alter any of our results. In fact, the deviation almost entirely disappears upon the thermodynamic integration, as can be seen from the curves of the Helmholtz free energy per particle F/k_BT, plotted in Fig. 13(b).

[1] S. C. Glotzer and M. J. Solomon, Nature Mater. **6**, 557 (2007).

[2] V. N. Manoharan, M. T. Elsesser, and D. J. Pine, Science **301**, 483 (2003).

[3] Y. Wang, Y. Wang, D. R. Breed, V. N. Manoharan, L. Feng, A. D. Hollingsworth, M. Weck, and D. J. Pine, Nature (London) **491**, 51 (2012).

[4] F. Romano, E. Sanz, and F. Sciortino, J. Chem. Phys. **134**, 174502 (2011).

[5] F. Romano, E. Sanz, and F. Sciortino, J. Phys. Chem. B **113**, 15133 (2009).

[6] E. G. Noya, C. Vega, J. P. K. Doye, and A. A. Louis, J. Chem. Phys. **132**, 234511 (2010).

[7] Z. Zhang, A. S. Keys, T. Chen, and S. C. Glotzer, Langmuir **21**, 11547 (2005).

[8] N. Kern and D. Frenkel, J. Chem. Phys. **118**, 9882 (2003).

[9] F. Smallenburg and F. Sciortino, Nature Phys. **9**, 554 (2013).

[10] D. de las Heras, J. M. Tavares, and M. M. Telo da Gama, Soft Matter **8**, 1785 (2012).

[11] O. A. Vasilyev, B. A. Klumov, and A. V. Tkachenko, Phys. Rev. E **88**, 012302 (2013).

[12] A. V. Tkachenko, Phys. Rev. Lett. **106**, 255501 (2011).

[13] J. D. Halverson and A. V. Tkachenko, Phys. Rev. E **87**, 062310 (2013).

[14] D. J. Evans, Mol. Phys. **34**, 317 (1977).

[15] D. J. Evans and S. Murad, Mol. Phys. **34**, 327 (1977).

[16] I. Saika-Voivod, F. Smallenburg, and F. Sciortino, J. Chem. Phys. **139**, 234901 (2013).

[17] T. P. Straatsma and H. J. C. Berendsen, J. Chem. Phys. **89**, 5876 (1988).

[18] P. J. Steinhardt, D. R. Nelson, and M. Ronchetti, Phys. Rev. Lett. **47**, 1297 (1981); Phys. Rev. B **28**, 784 (1983).

[19] I. Volkov, M. Cieplak, J. Koplik, and J. R. Banavar, Phys. Rev. E **66**, 061401 (2002).

[20] T. Aste, M. Saadatfar, A. Sakellariou, and T. J. Senden, Physica A **339**, 16 (2004); T. Aste, J. Phys.: Condens. Matter **17**, S2361 (2005).

[21] B. A. Klumov, S. A. Khrapak, and G. E. Morfill, Phys. Rev. B **83**, 184105 (2011).

[22] P. R. ten Wolde, M. J. Ruiz-Montero, and D. Frenkel, J. Chem. Phys. **104**, 9932 (1996).

[23] M. D. Rintoul and S. Torquato, J. Chem. Phys. **105**, 9258 (1996).

[24] W. Lechner and C. Dellago, J. Chem. Phys. **129**, 114707 (2008).

[25] B. A. Klumov, JETP Lett. **98**, 259 (2013); **97**, 327 (2013).

[26] G. E. Morfill, A. V. Ivlev, S. A. Khrapak, B. A. Klumov, M. Rubin-Zuzic, U. Konopka, and H. M. Thomas, Contrib Plasma Phys. **44**, 450 (2004).

[27] B. Klumov, P. Huber, S. Vladimirov, H. Ivlev, G. Morfill, V. Fortov, A. Lipaev, and V. Molotkov, Plasma Phys. Control. Fusion **51**, 124028 (2009).

[28] B. Klumov, G. Joyce, C. Räth, P. Huber, H. Thomas, G. E. Morfill, V. Molotkov, and V. Fortov, Europhys. Lett. **92**, 15003 (2010).

[29] B. A. Klumov, Phys. Usp. **53**, 1053 (2010).

[30] U. Gasser, E. R. Weeks, A. Schofield, P. N. Pusey, and D. A. Weitz, Science **292**, 258 (2001).

[31] T. Kawasaki and H. Tanaka, J. Phys.: Condens. Matter **22**, 232102 (2010).

[32] A. Hirata, L. J. Kang, T. Fujita, B. Klumov, K. Matsue, M. Kotani, A. R. Yavari, and M. W. Chen, Science **341**, 376 (2013).

[33] B. A. Klumov and G. E. Morfill, JETP Lett. **85**, 498 (2007); JETP **107**, 908 (2008).

[34] Y. Peng, Z. R. Wang, A. M. Alsayed, A. G. Yodh, and Y. Han, Phys. Rev. E **83**, 011404 (2011).